Real-time intraoperative fluorescence imaging system using light-absorption correction

George Themelis*
Technische Universität München
Institute for Biological and Medical Imaging
Arcisstrasse 21
80333 München, Germany
and
Helmholtz Zentrum München
Ingolstaedter Landstrasse 1
85764 Neuherberg, Germany

Jung Sun Yoo*
Technische Universität München
Institute for Biological and Medical Imaging
Arcisstrasse 21
80333 München, Germany
and
Helmholtz Zentrum München
Ingolstaedter Landstrasse 1
85764 Neuherberg, Germany
and
Seoul National University
Department of Physics and Astronomy
Frontier Physics Research Division & Biomedical Physics Laboratory
Seoul, Korea 151-747

Kwang-Sup Soh
Seoul National University
Department of Physics and Astronomy
Frontier Physics Research Division & Biomedical Physics Laboratory
Seoul, Korea 151-747

Ralf Schulz
Vasilis Ntziachristos
Technische Universität München
Institute for Biological and Medical Imaging
Arcisstrasse 21
80333 München, Germany
and
Helmholtz Zentrum München
Ingolstaedter Landstrasse 1
85764 Neuherberg, Germany

Abstract. We present a novel fluorescence imaging system developed for real-time interventional imaging applications. The system implements a correction scheme that improves the accuracy of epi-illumination fluorescence images for light intensity variation in tissues. The implementation is based on the use of three cameras operating in parallel, utilizing a common lens, which allows for the concurrent collection of color, fluorescence, and light attenuation images at the excitation wavelength from the same field of view. The correction is based on a ratio approach of fluorescence over light attenuation images. Color images and video is used for surgical guidance and for registration with the corrected fluorescence images. We showcase the performance metrics of this system on phantoms and animals, and discuss the advantages over conventional epi-illumination systems developed for real-time applications and the limits of validity of corrected epi-illumination fluorescence imaging. [DOI: 10.1117/1.3259362]

Keywords: fluorescence imaging; epi-illumination; light attenuation; intraoperative imaging; light absorption correction.

Paper 08367RR received Oct. 13, 2008; revised manuscript received Jul. 14, 2009; accepted for publication Sep. 16, 2009; published online Nov. 18, 2009.

1 Introduction

Fluorescence imaging can become an ideal modality for improving surgical procedures, since it relates directly to the surgeon's vision and offers attractive characteristics, including flexibility in generating contrast, high detection sensitivity, and portability. As a result, significant attention has been given toward identifying fluorescence imaging strategies that reveal surgical markers otherwise invisible to the naked eye, with applications ranging from improving tumor delineation,[1–5] sentinel lymph node identification, and metastasis staging,[6,7] to neuronal activity monitoring[8,9] or vascular mapping.[10,11] To fully capitalize on the potential of fluorescence for intraoperative applications, robust imaging technologies need to be developed for *in-vivo* imaging.

Fluorescence imaging of tissues can be compromised by the spatial variation of the tissue optical properties. This is because the fluorescence intensity collected depends nonlinearly on the tissue's optical properties. For example, highly absorbing lesions, such as highly vascularized tumors, may show darker than surrounding less-absorbing tissue, even if

*These authors contributed equally to this work.
Address all correspondence to: Vasilis Ntziachristos, Institute for Biological and Medical Imaging (IBMI), Technische Universität München & Helmholtz Zentrum München, Ingolstaedter Landstrasse 1, 85764 Neuherberg, Germany. Tel: +49 89 3187 3852; Fax: +49 89 3187 3017; E-mail: v.ntziachristos@tum.de.

1083-3668/2009/14(6)/064012/9/$25.00 © 2009 SPIE

they contain larger amounts of fluorochrome compared to the surrounding tissue.[12] Likewise, a semitransparent or nonabsorbing lesion such as a cyst or a lymph node may appear brighter than surrounding muscle tissue, even if both the cyst and the muscle contain the same fluorochrome concentration. The fluorescence intensity on an image has also a strong nonlinear dependence on the depth of the fluorescence activity. For example, a superficial fluorescent lesion will appear brighter than an identical lesion that is located deeper in tissue. Finally, tissue autofluorescence, i.e., the fluorescence emerging from native tissue fluorochromes such as collagen or NADH, may provide useful diagnostic information[13–15] but it can also reduce the contrast in visualizing exogenously administered fluorescence signals by yielding a nonspecific background signal.

Tomographic fluorescence imaging developed for *in-vivo* applications typically utilizes illumination and data collection along different projections and combines the measurements with mathematical descriptions of photon propagation in tissues to reconstruct images corrected for the effects of tissue optical heterogeneity and depth.[12,16] By using volumetric 3-D reconstructions, narrow bandpass filters, or appropriate subtraction methods, the effects of tissue autofluorescence can also be minimized. When considering real-time fluorescence imaging however, the application of multiprojection schemes and tomographic methods becomes challenging due to the scanning and computational times involved, which are generally significantly longer than video-rate speeds. Correspondingly, planar epi-illumination imaging approaches have been considered that cannot easily resolve depth but can lead to easy-to-implement video-rate imaging while offering correction for autofluorescence or the effects of optical property variation.[17–20] These methods suggest a computationally efficient processing of images acquired at two or more spectral bands, typically utilizing a form of ratio imaging, either between fluorescence measurements[18] or a combination of fluorescence and light attenuation images at the excitation or other wavelengths where the fluorochrome of interest does not fluoresce.[19,20] Besides the use of ratios, another strategy to reduce autofluorescence is to utilize near-infrared fluorochromes, since tissue autofluorescence in the near-infrared is much smaller compared to the visible.[21] In this case, increased penetration depth can be achieved compared to systems operating in the visible, due to the significantly lower attenuation of near-infrared light by tissues, compared to visible light.

In this work we consider the development of a novel fluorescence imaging system, operating in the near-infrared, which enables real-time operation and ratio-based image correction for heterogeneous light absorption in tissues, developed for intraoperative surgical imaging. The system's unique design allows the collection of three-channels, i.e., fluorescence, light absorption, and color images simultaneously, through one lens and the same field of view, while operating in real-time mode, i.e., at video-rate capacity of 25 fps. These data are then used to implement a previously developed fluorescence correction method,[16,20] which corrects the measurements at the emission (fluorescence) wavelength by dividing them with geometrically identical light attenuation measurements in tissue at the same or similar wavelengths, for example at the excitation wavelength. This approach has been shown to be capable of yielding accurate epi-illumination fluorescence images for at least a three-fold change of spatially varying absorption in the tissue imaged.[20] We showcase implementation aspects of this system and further demonstrate the performance achieved using phantoms and controlled postmortem mouse measurements. Taken together, the imaging of anatomy in the color channel combined with corrected fluorescence measurements using dual-channel imaging may provide the basis for accurate fluorescence epi-illumination imaging and video in a variety of interventional procedures, offering fluorescence quantification ability in real-time mode.

2 Methods

2.1 *System Design and Overview*

The key design parameters of the system developed were: 1. the capability of simultaneous video-rate imaging in NIR emission (fluorescence signals), NIR excitation (intrinsic signal), and visible wavelength bands; 2. the capability of providing image normalization; 3. operation at long working distances, large field of view, high detection sensitivity, and high resolution; and 4. a highly optimized detection sensitivity in all spectral bands considered.

To reach these functional specifications, a three-channel detection system was developed as shown in Fig. 1. The selection of three cameras is based on the need to use different camera specifications for color and near-infared (NIR) imaging while providing simultaneous readings of all the necessary measurements. The system specifications, as described in Sec. 3, are shown in Table 1. Illumination was provided by a 750-nm cw laser diode (BWF2-750-0, B and W Tek, Newark, Delaware; maximum power 300 mW) for fluorochrome excitation, and a 250-W halogen lamp (KL-2500 LCD, Edmund Optics, Barrington, New Jersey) for white-light color imaging. The system has the capacity to operate in epi-illumination and transillumination modes. Epi-illumination imaging was performed using a front illuminating expanded beam by guiding laser light through a multimode fiber (200-μm core/0.22 NA) to a collimator and a diffuser (F260SMA-B, ED1-S20, Thorlabs, Newton, New Jersey) for beam expansion and uniform illumination. White light was also coupled with a fiber optic bundle and homogenized by a beam expander (EG8546, Edmund Optics). Transillumination was accomplished by guiding laser light through a multimode fiber that was scanned on the bottom surface of the target, through an antireflection-coated glass window, using the x-y translation stage (MAXY4009Q1-S4, Velmex, Bloomfield, New York). Transillumination measurements were achieved using a diffuser in front of the multimode fiber to achieve more homogeneous back-illumination. x and y axes were scanned with four steps of 35 mm and three steps of 33.75 mm, respectively.

Light from the surgical field was collected using a zoom lens (NT58-240, Edmund Optics). Linear polarizers were employed for minimizing the effects of glare and specular reflection in the attenuation and color images by enabling cross-polarized measurements for white and excitation (intrinsic) light measurements. The additional advantage of polarization is that it samples deeper into tissue compared to nonpolarized imaging, which is an important parameter in getting a more accurate reading on tissue attenuation in epi-illumination

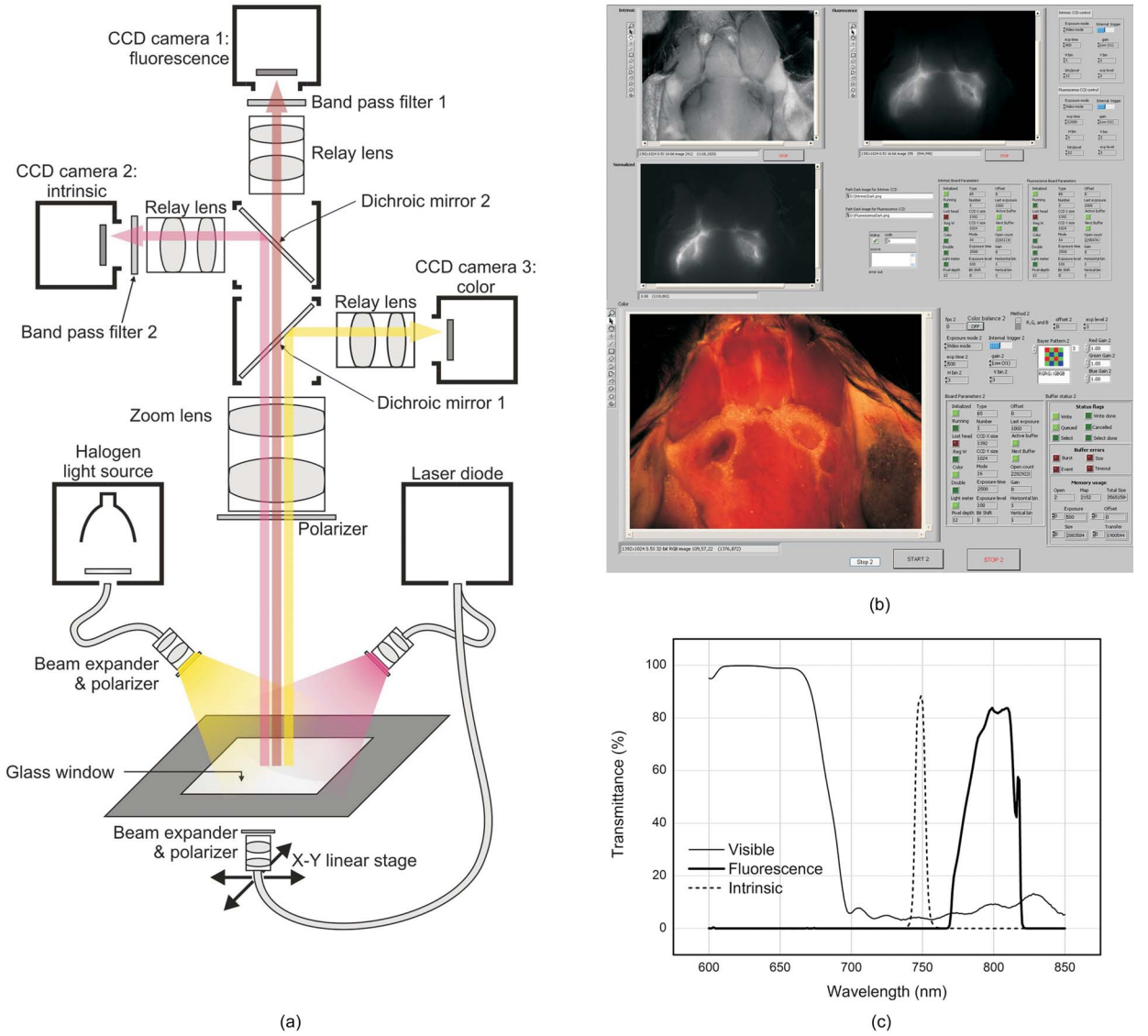

Fig. 1 (a) Schematic of the imaging system developed to operate in real-time (video) mode and implementing concurrent fluorescence, attenuation (intrinsic), and color measurements. All optical path lengths from the lens to the cameras are equal (not plotted in scale on the drawing). Three CCDs and the linear stage are under computer control. (b) Imaging windows display and user interface for operational guidance. Measurements at excitation (intrinsic) and emission wavelength, and corresponding normalized fluorescence image are shown. (c) Spectra of light transmittance in each imaging channel. Clear separation of wavelength for visible and near-infrared is originated from the combination of dichroic mirror and bandpass filters.

mode. However, when switching to imaging through the cross-polarizers, lower resolution is generally achieved. This feature is used selectively when specular reflection indeed occurs.

The primary image of the object formed by the zoom lens falls at the focal plane of each relay lens group (MAP10100100-A1, Thorlabs) of three imaging channels. The setup employs two dichroic mirrors (700 DCXXR, z 750 RDC, Chroma, Rockingham, Vermont) that splits light by excitation, emission, and visible wavelengths into three imaging channels. The final images are formed on each chip surface of a 12-bit grayscale charge-coupled device (CCD) camera with 20% quantum efficiency in the NIR area and a 24-bit color CCD camera (PCO AG, Donaupark, Kelheim, Germany) by each relay lens group. This relay lens group has the same object and image distance, so it does not change the magnification. Its purpose is the delivery of the primary image from the lens to each CCD chip, while allowing the intersection of dichroic mirrors, filters, and potentially other imaging components. All optical pathlengths from the lens to the cameras are equal (not plotted in scale in Fig. 1). For accurate wavelength-band selection and cross talk elimination, bandpass filters (z 750/10, HQ 795/50, Chroma) were used in front of CCD cameras in excitation (intrinsic) and emission imaging channels. The transmission spectrum of each imaging channel, which is induced by the combination of dichroic mirrors and the bandpass filter, can be seen in Fig. 1(c). For implementing a portable self-contained system, all optical components were tightly mounted in custom coupler/holders via C-mount optics after exact optical alignment.

Table 1 Imaging system specifications.

Physical size of imaging module	455 W×62 D×415 H (mm)
Zoom ratio	6:1
Working distance	210 mm
Surgical field of view	13.5 W×11 H (mm) to 115 W×93 H (mm)
Primary magnification	0.73 X–0.09 X
Sensor resolution (spatial)	1392 W×1024 H (pixel), pixel size 6.45 μm^2
Sensor resolution (temporal)	12 fps (full frame), 23 fps (binning 2Xver)
Image windows	Visible, fluorescence, intrinsic, normalized

The control software and user interface for surgical guidance was developed under the LabVIEW (National Instruments, Austin, Texas) and Matlab (The MathWorks, Natick, Massachusetts) environments. In continuous acquisition mode, NIR excitation (intrinsic), NIR emission (fluorescence), and anatomical color image can be displayed simultaneously in real time and refreshed continuously at a rate set by the camera exposure time using two computers. In a single snap acquisition mode, when a set of images is captured, then instantly the normalized fluorescence image is calculated and displayed, as shown in Fig. 1(b). The user interface provides complete control on the imaging system including camera gain, exposure time, number of binning, image display, and image archiving.

2.2 *Measurement of Optical Resolution*

To measure the spatial resolution of the system, the image of a standard three-bar resolving power test target (USAF-1951, NT53-714, Edmund Optics) was taken using the visible wavelength channel and white-light illumination. This target contains numbered bar groups, each consisting of three vertical and three horizontal bar patterns. The ratio of the spatial frequency of an element to the one of the next higher element is $1:2^{1/6}$. After extraction of cross-sectional intensity profiles from each horizontal and vertical bar element, the points of the contrast transfer function (CTF) are obtained with the contrast equation, i.e.,

$$\mathrm{CTF}(f) = \frac{I_{\max}(f) - I_{\min}(f)}{I_{\max}(f) + I_{\min}(f)}, \tag{1}$$

where $I_{\max}$ and $I_{\min}$ are the maximum and minimum gray values of adjacent line patterns, and f is the number of line pairs per millimeter (lines/mm), which shows corresponding spatial frequency for each bar element.

2.3 *Phantoms*

To examine the metrics of fluorescence quantification correction as it relates to spatial variations of excitation light in tissue, we constructed a phantom consisting of five tubes containing the same fluorochrome concentration but different concentrations of absorbing dye, resulting in variation in the underlying optical properties. The five tubes were made of translucent ~3-mm-diam plastic and contained 400 nM of Alexa Fluor 750 dye (Molecular Probes, Eugene, Oregon) and 1% Intralipid solution. In addition, the tubes contained India ink of varying concentration from 50 to 250 ppm with 50-ppm increments to impart differences in attenuation between tubes. The imaging chamber had an open upper surface, whereas its bottom surface was a glass window, which was antireflection coated for the NIR to facilitate both epi-illumination and transillumination measurements. The tubes were placed in an imaging chamber and positioned parallel to each other, allowing a 6-mm gap between consecutive tubes. The chamber was filled with 1% Intralipid solution (Sigma, Saint, Louis, Missouri) and 50-ppm India ink (yielding optical properties of absorption coefficient $\mu_a = 0.4\ \mathrm{cm}^{-1}$ and reduced scattering coefficient $\mu_s' = 8\ \mathrm{cm}^{-1}$, characteristic of small animals). The thickness of the fluid phantom was 1 cm and the tops of all the tubes were positioned 2 mm below the top surface of the fluid solution. A similar phantom containing a single tube was also constructed and was employed to examine the effects of background absorption variation. A single tube was immersed in the Intralipid solution, and the absorption of the Intralipid solution was altered by titrating India ink (50 to 250 ppm) in the solution that surrounded the tissue.

2.4 *Tissue Imaging*

Euthanized mice (C57BL/6J, n=4) were employed to showcase imaging feasibility simulating intraoperative imaging. After euthanasia, the abdominal sides of the mouse were surgically exposed, and the lumbar nodes beside the inferior vena cava were visualized by removing the surrounding peritonea and fat. Imaging of the nodes was selected because it allows for visualizing well defined volumes. 8 μM of Alexa Fluor 750 with 300 ppm of India ink was injected into one lymph node and the same fluorescent solution, and without ink into another lymph node (10 μl for each node), using a 30-gauge needle.

2.5 *Measurements and Normalization*

The correction scheme considered assumes a raw fluorescence image I in epi-illumination or transillumination modes, i.e.,

$$I = I_f - I_d, \tag{2}$$

where I_f is the raw fluorescence image and I_d is the dark current image, respectively. We also examined the corresponding images after normalization with the light attenuation (intrinsic) images acquired. The corresponding normalized image U can be written as

$$U = \frac{I_f - I_d}{(I_{if} - I_{id})_{>T_i}}, \tag{3}$$

where I_{if} is the light attenuation image obtained at the excitation wavelength (intrinsic image), and I_{id} is the corresponding dark current image obtained with no illumination for the same acquisition parameters used for I_{if}. We set U to zero

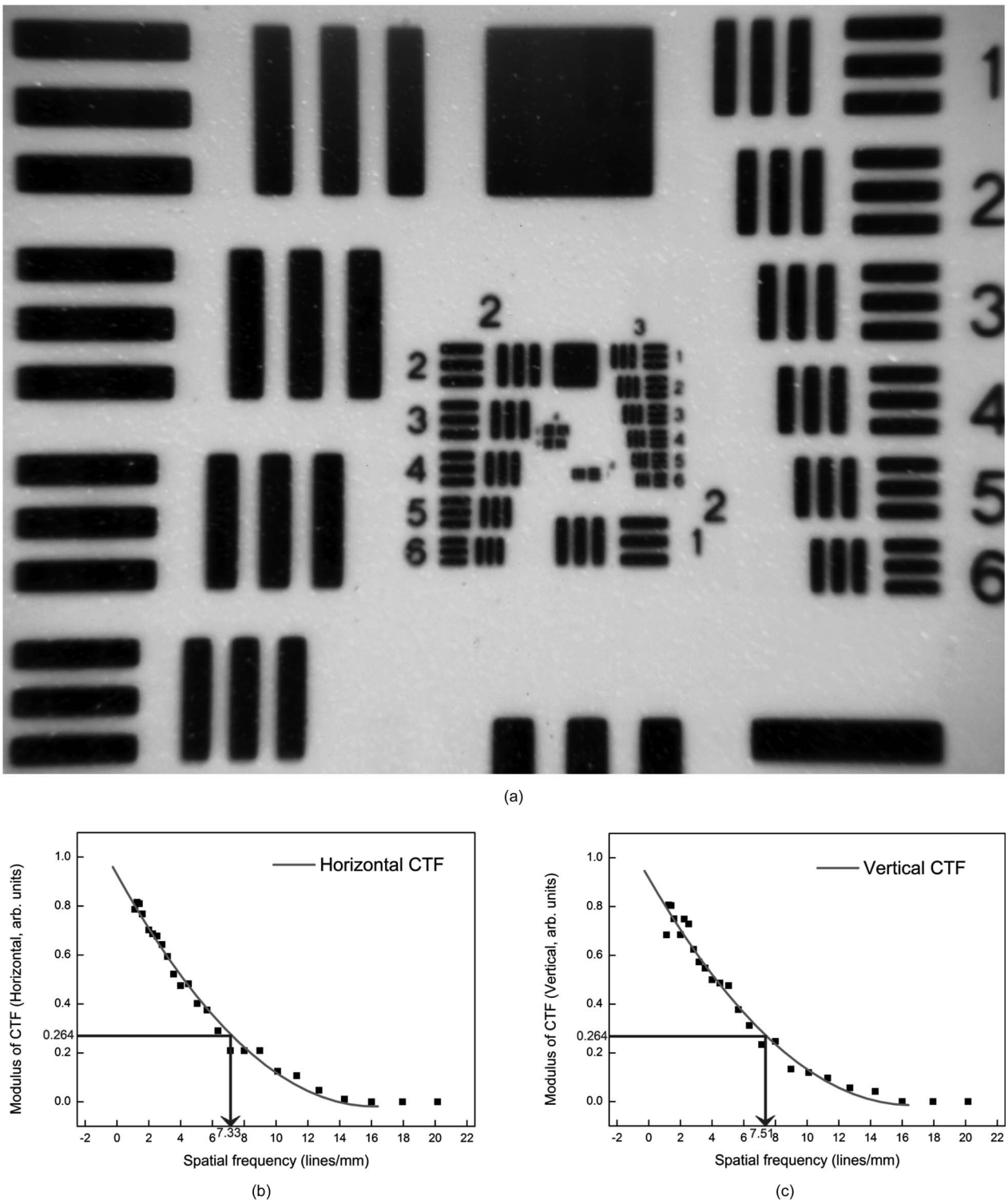

Fig. 2 Spatial resolution of the implemented imaging system. (a) Color video image of a U.S. Air Force 1951 standard resolution target was taken. (b) and (c) Horizontal and vertical contrast transfer function are obtained by determining the specific contrast produced by bar group patterns of various spatial frequencies [see Eq. (1)]. By using a CTF fitting curve [solid black lines in (b) and (c)] the transverse resolution of the system was measured as 68.21 and 36 μm by the Rayleigh criterion (26.4% contrast) and the Sparrow criterion (0% contrast), respectively. Similarly, the lateral resolution of the system was determined to be 66.58 and 34 μm by the Rayleigh criterion and the Sparrow criterion, respectively. Use of a different front lens can increase the resolution but limit the field of view.

unless the denominator values are above a threshold T_i, typically set to 5% of the maximum of the denominator values to avoid divisions with very small noise-affected values. In transillumination mode, all fluorescence and attenuation images obtained from the light source scanning are summed up after subtraction with the noise (dark current) images I_d and I_{id} to show the whole field of view.

3 Results

3.1 *Resolution*

The spatial resolution of the implemented system was determined utilizing the USAF-1951 pattern target image and contrast transfer function (CTF) as shown in Fig. 2. The test pattern image consisting of repeated gratings is obtained at visible wavelength channels with the highest zoom setting [Fig. 2(a)]. For every different grating size in the field of view, we calculated the CTF parameter using Eq. (1). Figures 2(b) and 2(c) illustrate the CTF values (vertical axis) versus the different grating frequencies (horizontal axis).

Figures 2(b) and 2(c) show the contrast transfer function in the image plane as a function of the spatial frequency f along the horizontal and vertical directions, respectively. To quantify the transverse or lateral resolution of the system, we applied the Rayleigh criterion and the Sparrow criterion to the profiles measured from the phantom by the system developed. The Rayleigh criterion defines resolution as the distance between two point objects, where the Airy disk minimum of the image of one object coincides with the maximum of the Airy disk of the other object. Typically at this limit the contrast between the maximum and minimum intensity observed between the two objects becomes about 26.4%. The Sparrow criterion defines the resolution of an optical system as being equal to the cut-off distance, i.e., the distance below which two objects cannot be distinguished by means of contrast. Since the line pair corresponding to a contrast value of 26.4% was 7.33 and 7.51 lp/mm in the horizontal and vertical CTF curves, respectively, by taking the half-width between two line pairs we determined the transverse resolution of the system to be 68.21 μm and the lateral resolution to be 66.58 μm by the Rayleigh criterion. Correspondingly, the transverse and the lateral resolutions of the system by the Sparrow criterion were found to be 36 and 34 μm, respectively. Since three imaging channels are constructed with identical optical components and pathways, the resolution characteristics were similar in all channels with minor variations (<5 μm), largely due to wavelength-dependent characteristics of the optical components utilized.

3.2 *Epi-Illumination Imaging*

Figure 3 shows the results obtained in epi-illumination from the fluid phantom containing the five tubes of identical fluorochrome concentration but of varying attenuation, simulating tissue optical heterogeneity. Figure 3(a) depicts the image obtained at the excitation wavelength (intrinsic image). A characteristic pattern of varying light absorption by the tubes is visible, in an increasing fashion from tube 1 to tube 5, due to the increasing concentration of the absorber. The uncorrected fluorescence image in Fig. 3(b) shows the dependency of the fluorescence signal on the varying absorption in the tubes, and demonstrates correspondingly a decreasing fluorescence signal with increasing tube attenuation. In this case, while all the tubes have the same fluorescence concentration, the image reports varying fluorescence intensity that could be erroneously interpreted as changes in the amount of fluorescence present in the tubes. In contrast, the normalized fluorescence image shown in Fig. 3(c) correctly depicts a similar fluorescence strength from all tubes by correcting the effects of background attenuation. In addition, it shows a better delineation of the tubes compared to the uncorrected images. Finally, the images demonstrate very low specula reflection, as it is successfully eliminated by means of the cross-polarized linear polarizers employed in the system.

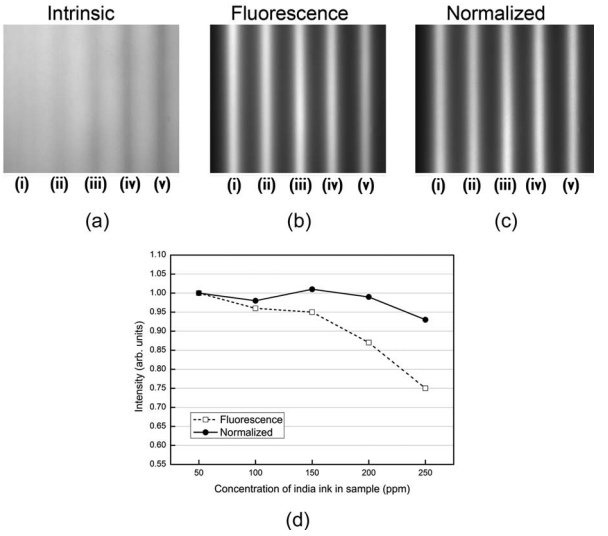

Fig. 3 Epi-illumination imaging performance from a phantom of five fluorescence tubes immersed in a diffusive fluid as a function of absorption variation in the tubes shown. (a) Attenuation (intrinsic) image at the excitation wavelength, (b) the fluorescence image, and (c) the corresponding normalized fluorescence image. All images were acquired simultaneously. (d) Intensity strength ratio for the five tubes imaged, for normalized and conventional fluorescence measurements.

To quantitatively determine the differences between nonnormalized and normalized images, the average photon counts in all tubes were calculated over identical regions of interest during image post-processing. The region of interest was chosen as an area spanning the length of the tube and a width of 30 pixels, with the center being the center of the tube. The ratio graph in Fig. 3(d) indicates that the quantification performance of the normalized fluorescence image is significantly better than in the standard epi-illumination image, the latter showing signal variations as high as 25%.

Figure 4 correspondingly depicts the quantification results between corrected and uncorrected fluorescence imaging when the absorption of the background was changed. As can be seen, changes in the background also affect the signal recorded, as expected, and in this case again the corrected approach yields better insensitivity to the variation of light attenuation.

3.3 *Transillumination Imaging*

Figure 5 depicts the transillumination imaging results obtained from the same phantom as in Fig. 3. In transillumina-

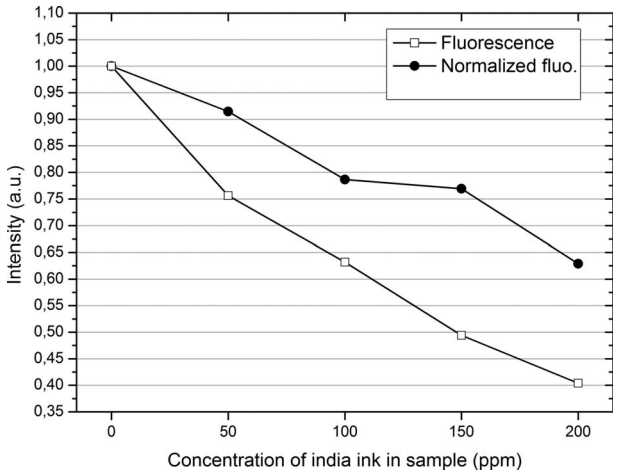

Fig. 4 Epi-illumination imaging performance from a single tube phantom as a function of absorption variation in the diffusive medium that surrounds the tube. Corrected images show again better insensitivity to the effects of increasing background attenuation compared to uncorrected images.

tion, the light propagates through the entire volume of the tubes. This generally leads to more prominent variations of signal intensity compared to epi-illumination, since a larger optically heterogeneous volume is sampled. Figures 5(a) and 5(b) depict the raw data obtained in the excitation and emission wavelengths, respectively. The fluorescence signal intensity varies significantly in the uncorrected image. In contrast, Fig. 5(c) depicts the normalized image showing a significantly more homogenous response from the fluorescent tubes. Finally, the chart shown in Fig. 5(d) summarizes the imaging

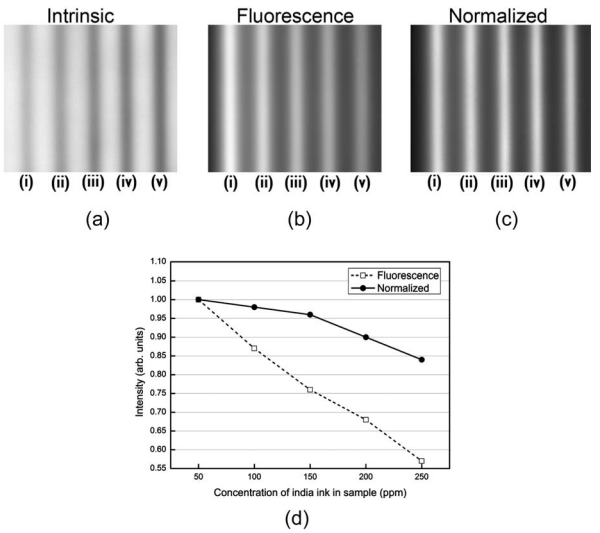

Fig. 5 Transillumination imaging with varying background optical properties. (a) Attenuation (intrinsic) image at the excitation wavelength, (b) the fluorescence image, and (c) the corresponding normalized fluorescence image. (d) Intensity strength ratio for the five tubes imaged, for normalized and conventional fluorescence measurements. The normalized transillumination image reveals the robustness on optical property variation, while the standard transillumination image reports significant error as the concentration of India ink is increased from tube 1 to tube 5.

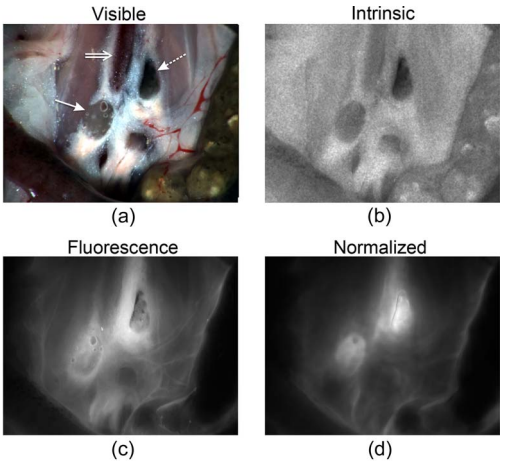

Fig. 6 Postmortem imaging of the surgically exposed mouse abdominal area in epi-illumination mode. (a) Color image showing the lumbar lymph nodes (single-line arrows) around the inferior vena cava (double arrow). (b) Image obtained at the excitation wavelength (intrinsic image) depicts absorption differences between the two lymph nodes due to the differential injection of an absorber. (c) Conventional fluorescence image showing low signal intensity from the lymph nodes compared to bright background signals. (d) Normalized image showing markedly improved fluorescence quantification, correctly resolving the underlying fluorescence activity in the nodes. (Color online only.)

results. It can be observed that the quantification performance of normalized transillumination imaging is significantly better than the uncorrected transillumination image. Especially for absorption values up to 3× of the reference sample, the error of normalized imaging is less than 5% while the corresponding error for uncorrected transillumination images reaches 24%.

3.4 *Tissue Imaging*

While Figs. 3–5 demonstrate general performance metrics obtained from measurements on phantoms, Fig. 6 depicts epi-illumination images obtained from a mouse after euthanasia and surgical exposure of the abdominal area. In this case, two lymph nodes were injected with solutions of identical fluorochrome concentration but different absorption to simulate varying tissue optical properties, as described in Sec. 2. This model could be relevant to real-time pathology studies, where nodes are sampled for achieving real-time intraoperative pathology, but it is more generally used here to obtain performance metrics using tissues.

Figure 6(a) shows a color image obtained from the field of view using the color video camera. This view closely relates to the surgeon's field of view and it is important for reference purposes. The inferior vena cava (double arrow) and two lumbar nodes (single-line arrows) are seen on the color figure. Figures 6(c) and 6(d) depict the attenuation (intrinsic), fluorescence, and normalized fluorescence images, respectively. Although the same concentration of fluorochrome was injected in both lymph nodes, the right lymph node (dotted line arrow) was darker (i.e., more attenuating) compared to the left node (solid line arrow), as identified in Fig. 6(b). Figure 6(c) is the uncorrected fluorescence image that shows fluorescence activity from areas surrounding the node. This behavior has

been previously documented[20] and is likely due to escaping photons from the node toward the lower attenuating surrounding tissue. From an imaging standpoint this is an erroneous result, as it indicates that the fluorescence dye was injected in the tissue surrounding the node. Conversely, the normalized image of Fig. 6(d) depicts a significantly more accurate picture of fluorescence biodistribution and correctly resolves the nodes as the areas of fluorescence origin.

These images further confirm the observations of Figs. 3–5, where the measured fluorescence intensity did not depend only on the fluorochrome concentration but also on the heterogenous attenuation of light in the underlying tissue. It also further showcases that the spatial appearance and contrast of the image also improves when the fluorescence image is corrected for the underlying optical properties. In that respect, correction can lead to a more accurate and robust performance.

4 Discussion

The propagation of fluorescence imaging into interventional procedures requires a modality that is robust and reliable, independent of tissue optical parameters or illumination variations. While often unappreciated in epi-illumination imaging, the light intensity incident on the surface is spatially modulated by optical properties, which in turn modulate the fluorescence intensity in an unknown fashion unless explicitly measured and used to correct the corresponding fluorescence images.

We developed a system appropriate for real-time intraoperative imaging that employs a three-channel imaging approach, used to deliver color real-time video imaging as well as corrected (normalized) fluorescence images. This approach is offered as an alternative to simple "photographic" fluorescence imaging or video, and leads to improved accuracy independently of optical property variation in tissues, as demonstrated here with phantoms and tissues postmortem. In particular, we found that the system allows quantification errors of less than 8%, even at a five-fold change of absorption variation within the fluorescent lesion, whereas uncorrected images show errors of 25%. In transillumination, image correction yielded 16% quantification error versus 45% for the uncorrected image. Finally, when the background absorption was varied by three-fold, the corresponding errors recorded were 35 and 60% for corrected and uncorrected images, respectively. Overall, the performance of corrected (normalized) images shows significant insensitivity over a wide variation of background absorption versus the uncorrected images. This performance is particularly important, for example, when imaging highly vascular, nonvascular, or more general areas with variations in hemoglobin concentration, i.e., the major light absorber in tissue. This performance is also relevant to volumetric sampling of tissues, i.e., in imaging entire tissue masses or nodes using transillumination with a small catheter illuminator,[22] since the correction applied is particularly well suited for improving the quantification and overall image quality in transillumination images as well.

It should be noted that since the system utilizes light of constant intensity, it is insensitive in sensing whether a spatial light attenuation variation is due to absorbing or scattering variations. Illumination and detection of light of constant intensity (in contrast to using intensity modulation or ultrafast pulsing technologies[12]) is a common technology applied to intraoperative imaging, as it leads to the use of practical and economic systems.[3,4,6,9,19,23] However, in contrast to the insensitivity of the ratio to spatial changes of the absorption coefficient, the ratio of fluorescence to intrinsic intensity scales with tissue scattering is a factor of $\sim 3\mu_s'/4\pi$.[16] Therefore, although the method can accurately improve fluorescence quantification in cases of tissue vascularization changes, more advanced technologies such as frequency domain[24] or time-resolved approaches will be important for decomposing absorption from scattering effects and for better application of the ratio correction when strong scattering variation is present in the tissues. Such systems should still correct for the variation of optical property in tissues, before yielding accurate quantification of surface and subsurface fluorescence activity, using the known dependency of the ration on scattering variations as well. It should be also be pointed out that the division of Eq. (3) also corrects for inhomogeneous illumination due to imperfect beam shape or light obstacles that may interfere with the illumination, since they multiply both intrinsic and fluorescence measurements and therefore are exactly cancelled out by a ratio approach.

There is a strong dependence of imaging performance on depth. This dependence has been studied in the past[20,25] in the context of analyzing the performance of the method implemented here by the proposed system. For deeper seated fluorescence activity, the correction advantages proposed are only possible in transillumination mode. This is because the use of the "intrinsic signal" measurement for correction is appropriate only in the first 1 to 2 mm of depth, where relevant light attenuation contrast is present. This is the reason why the system has also a developed transillumination branch. The premise is that for deeper seated activity or large tissue volumes, the surgeon would be able to direct focused illumination from a certain angle (projection) into tissue, using a catheter system, instead of using wide-plane epi-illumination. Light diffusion in this case plays the role of "beam expansion" in the tissue, and a larger or deeper volume of tissue can be sampled in this way. It was also shown in mice that this approach offers significant betterment compared to uncorrected fluorescence patterns.[20]

The increasing availability of fluorescent probes with enhanced *in-vivo* sensitivity and specificity to molecular disease markers makes fluorescence imaging a very appealing method for real-time intraoperative visualization of invasive tumor borders and local metastatic foci. The fluorescence concentration values utilized here have been drawn from typical *in-vivo* animal measurements. The ability to detect with high sensitivity fluorescence distributed in tissues has been amply demonstrated in the literature using highly sensitive CCD cameras appropriate for low light imaging. Overall the detection performance of such system is of the order of a few tenths of femptomoles or better for typical organic fluorescent dyes operating in the NIR.[12] Using the previous normalization technique, fluorescence imaging can become a robust imaging technique that is insensitive to tissue optical heterogeneity and illumination variations. While quantitative volumetrical sampling can be better achieved by fluorescence molecular tomography[12] or multispectral optoacoustic tomography

(MSOT),[26,27] these techniques require time-consuming scanning and computation that is not appropriate for real-time imaging. The system presented can work synergistically with other methods, such as intraoperative radiological or nuclear medicine methods to offer an integrated solution of macroscopic noninvasive imaging combined with high resolution invasive imaging. Using different magnifications, the same system can be used for fluorescence inspection of the field of view and then zoomed in for high resolution imaging of regions of interest. Likewise the basic setup developed could be used as the back end of a surgical microscope or endoscope system. In addition, by using different spectral areas, multiple fluorescence probes can be further resolved to improve the information available to the surgeon. We have recently developed a multispectral approach for true real-time imaging,[28] and we are currently considering its implementation with the correction system and strategy presented. Overall we expect that quantitative normalized fluorescence imaging will become an important intraoperative enhancement in improving surgical vision.

Acknowledgments

The author's acknowledge useful discussions with Go Van Dam. In addition to institutional funding, this work was further supported by the DFG grant MOBITUM. Jung Sun Yoo was supported by the Korea Research Foundation Grant funded by the Korean government (MOEHRD, KRF-2007-612-C00046).

References

1. T. Kuroiwa, Y. Kajimoto, and T. Ohta, "Development of a fluorescein operative microscope for use during malignant glioma surgery: a technical note and preliminary report," *Surg. Neurol.* **50**, 41–49 (1998).
2. W. Stummer, A. Novotny, H. Stepp, C. Goetz, K. Bise, and H. J. Reulen, "Fluorescence-guided resection of glioblastoma multiforme by using 5-aminolevulinic acid-induced porphyrins: a prospective study in 52 consecutive patients," *J. Neurosurg.* **93**, 1003–1013 (2000).
3. M. F. Kircher, U. Mahmood, R. S. King, R. Weissleder, and L. Josephson, "A multimodal nanoparticle for preoperative magnetic resonance imaging and intraoperative optical brain tumor delineation," *Cancer Res.* **63**, 8122–8125 (2003).
4. W. Stummer, T. Beck, W. Beyer, J. H. Mehrkens, A. Obermeier, N. Etminan, H. Stepp, J. C. Tonn, R. Baumgartner, J. Herms, and F. W. Kreth, "Long-sustaining response in a patient with non-resectable, distant recurrence of glioblastoma multiforme treated by interstitial photodynamic therapy using 5-ALA: case report," *J. Neuro-Oncol.* **87**, 103–109 (2008).
5. P. S. Adusumilli, B. M. Stiles, M. K. Chan, D. P. Eisenberg, Z. Yu, S. F. Stanziale, R. Huq, R. J. Wong, V. W. Rusch, and Y. Fong, "Real-time diagnostic imaging of tumors and metastases by use of a replication-competent herpes vector to facilitate minimally invasive oncological surgery," *FASEB J.* **20**, 726–728 (2006).
6. D. P. Eisenberg, P. S. Adusumilli, K. J. Hendershott, S. Chung, Z. Yu, M. K. Chan, M. Hezel, R. J. Wong, and Y. Fong, "Real-time intraoperative detection of breast cancer axillary lymph node metastases using a green fluorescent protein-expressing herpes virus," *Ann. Surg.* **243**, 824–832 (2006).
7. E. Tanaka, H. S. Choi, H. Fujii, M. G. Bawendi, and J. V. Frangioni, "Image-guided oncologic surgery using invisible light: completed pre-clinical development for sentinel lymph node mapping," *Ann. Surg. Oncol.* **13**, 1671–1681 (2006).
8. M. M. Haglund and D. W. Hochman, "Imaging of intrinsic optical signals in primate cortex during epileptiform activity," *Epilepsia* **48**(Suppl 4), 65–74 (2007).
9. K. Sato, T. Nariai, S. Sasaki, I. Yazawa, H. Mochida, N. Miyakawa, Y. Momose-Sato, K. Kamino, Y. Ohta, K. Hirakawa, and K. Ohno, "Intraoperative intrinsic optical imaging of neuronal activity from subdivisions of the human primary somatosensory cortex," *Cereb. Cortex* **12**, 269–280 (2002).
10. E. N. Brown, N. S. Burris, J. Gu, Z. N. Kon, P. Laird, S. Kallam, C. M. Tang, J. M. Schmitt, and R. S. Poston, "Thinking inside the graft: applications of optical coherence tomography in coronary artery bypass grafting," *J. Biomed. Opt.* **12**(5), 051704 (2007).
11. A. Nakayama, F. del Monte, R. J. Hajjar, and J. V. Frangioni, "Functional near-infrared fluorescence imaging for cardiac surgery and targeted gene therapy," *Mol. Imaging* **1**, 365–377 (2002).
12. V. Ntziachristos, J. Ripoll, L. V. Wang, and R. Weissleder, "Looking and listening to light: the evolution of whole-body photonic imaging," *Nat. Biotechnol.* **23**, 313–320 (2005).
13. N. Thekkek and R. Richards-Kortum, "Optical imaging for cervical cancer detection: solutions for a continuing global problem," *Nat. Rev. Cancer* **8**, 725–731 (2008).
14. D. C. de Veld, M. Skurichina, M. J. Witjes, R. P. Duin, H. J. Sterenborg, and J. L. Roodenburg, "Autofluorescence and diffuse reflectance spectroscopy for oral oncology," *Lasers Surg. Med.* **36**, 356–364 (2005).
15. I. Georgakoudi and M. S. Feld, "The combined use of fluorescence, reflectance, and light-scattering spectroscopy for evaluating dysplasia in Barrett's," *Gastrointest Endosc Clin. N. Am.* **14**, 519–537 (2004).
16. V. Ntziachristos and R. Weissleder, "Experimental three-dimensional fluorescence reconstruction of diffuse media by use of a normalized Born approximation," *Opt. Lett.* **26**, 893–895 (2001).
17. D. Zaak, D. Frimberger, H. Stepp, S. Wagner, R. Baumgartner, P. Schneede, M. Siebels, R. Knuchel, M. Kriegmair, and A. Hofstetter, "Quantification of 5-aminolevulinic acid induced fluorescence improves the specificity of bladder cancer detection," *J. Urol. (Baltimore)* **166**, 1665–1669 (2001).
18. V. X. Yang, P. J. Muller, P. Herman, and B. C. Wilson, "A multispectral fluorescence imaging system: design and initial clinical tests in intra-operative Photofrin-photodynamic therapy of brain tumors," *Lasers Surg. Med.* **32**, 224–232 (2003).
19. A. Bogaards, H. J. Sterenborg, J. Trachtenberg, B. C. Wilson, and L. Lilge, "In vivo quantification of fluorescent molecular markers in real-time by ratio imaging for diagnostic screening and image-guided surgery," *Lasers Surg. Med.* **39**, 605–613 (2007).
20. V. Ntziachristos, G. Turner, J. Dunham, S. Windsor, A. Soubret, J. Ripoll, and H. A. Shih, "Planar fluorescence imaging using normalized data," *J. Biomed. Opt.* **10**(6), 064007 (2005).
21. M. G. Muller, I. Georgakoudi, Q. Zhang, J. Wu, and M. S. Feld, "Intrinsic fluorescence spectroscopy in turbid media: disentangling effects of scattering and absorption," *Appl. Opt.* **40**, 4633–4646 (2001).
22. M. Niedre and V. Ntziachristos, "Elucidating structure and function in vivo with hybrid fluorescence and magnetic resonance imaging," *Proc. IEEE* **96**, 382–396 (2008).
23. J. V. Frangioni, "New technologies for human cancer imaging," *J. Clin. Oncol.* **26**, 4012–4021 (2008).
24. J. P. Houston, A. B. Thompson, M. Gurfinkel, and E. M. Sevick-Muraca, "Sensitivity and depth penetration of continuous wave versus frequency-domain photon migration near-infrared fluorescence contrast-enhanced imaging (vol 77, pg 420, 2003)," *Photochem. Photobiol.* **78**, 103 (2003).
25. J. Ripoll, D. Yessayan, G. Zacharakis, and V. Ntziachristos, "Experimental determination of photon propagation in highly absorbing and scattering media," *J. Opt. Soc. Am. A Opt. Image Sci. Vis* **22**, 546–551 (2005).
26. D. Razansky, C. Vinegoni, and V. Ntziachristos, "Multispectral photoacoustic imaging of fluorochromes in small animals," *Opt. Lett.* **32**, 2891–2893 (2007).
27. D. Razansky, M. Distel, C. Vinegoni, R. Ma, N. Perrimon, R. Koester, and V. Ntziachristos, "Multispectral opto-acoustic tomography of deep-seated fluorescent proteins in vivo," *Nat. Photonics* **3**, 412–417 (2009).
28. G. Themelis, J. S. Yoo, and V. Ntziachristos, "Multispectral imaging using multiple-bandpass filters," *Opt. Lett.* **33**, 1023–1025 (2008).